Electronic Structure of Metal Chalcogen Cubane Clusters: Photoelectron Spectroscopic, Electrochemical, and Theoretical Studies of $[(\eta\text{-}C_5H_4Me)TiS]_4$, $[(\eta\text{-}C_5H_4Me)VS]_4$, $[(\eta\text{-}C_5H_5)CrO]_4$, $[(\eta\text{-}C_5H_4Me)CrO]_4$, $[(\eta\text{-}C_5H_4Me)CrS]_4$, $[(\eta\text{-}C_5H_4Me)CrSe]_4$, $[(\eta\text{-}C_5H_4{}^iPr)MoS]_4$, and $[(\eta\text{-}C_5H_4{}^iPr)MoSe]_4$

Cathryn E. Davies,[†] Jennifer C. Green,*[,†] Nikolas Kaltsoyannis,[†] Michael A. MacDonald,[‡] Jingui Qin,[†] Thomas B. Rauchfuss,[§] Catherine M. Redfern,[†] Graham H. Stringer,[†] and Mark G. Woolhouse[†]

Inorganic Chemistry Laboratory, South Parks Road, Oxford OX1 3QR, U.K., SERC Daresbury Laboratory, Daresbury, Warrington WA4 4AD, U.K., and School of Chemical Sciences, University of Illinois, Urbana, Illinois 61801

Received January 24, 1992

He I and He II spectra of $[(\eta\text{-}C_5H_4{}^iPr)MoS]_4$, $[(\eta\text{-}C_5H_4{}^iPr)MoSe]_4$, $[(\eta\text{-}C_5H_4Me)CrS]_4$, $[(\eta\text{-}C_5H_4Me)CrSe]_4$, $[(\eta\text{-}C_5H_4Me)TiS]_4$, $[(\eta\text{-}C_5H_4Me)VS]_4$, $[(\eta\text{-}C_5H_5)CrO]_4$, and $[(\eta\text{-}C_5H_4Me)CrO]_4$ are presented. The photoelectron spectrum of $[(\eta\text{-}C_5H_4{}^iPr)MoS]_4$ has been measured using synchrotron radiation over the photon energy range 21–80 eV. Relative partial photoionization cross section and photoelectron branching ratio data are presented for the first six valence bands (binding energy 5.0–10.5 eV). The cross sections of the d bands show a p → d giant resonance in the photon energy range 39–60 eV. Intensity variations are interpreted in terms of the atomic orbital contributions to the molecular orbitals from which ionization is occurring. Similarities are observed between the low binding energy (4.8–7.5 eV) regions of the spectra of the sulfur and selenium derivatives of the group 6 elements and are interpreted in terms of ionization from molecular orbitals, composed largely of metal d-orbitals, delocalized over the metal tetrahedron. The molecular ion state ordering $^2T_2 < {}^2E < {}^2A_1$ is observed, the $^2T_2$ and ^2E states showing Jahn–Teller splitting. The a_1 and e orbitals are metal–metal bonding whereas the t_2 orbitals are nonbonding. Subsequent bands are assigned to cyclopentadienyl π orbitals and to metal–chalcogen bonding orbitals. The spectrum of $[(\eta\text{-}C_5H_4Me)VS]_4$ is consistent with an $a_1{}^2e^4t_2{}^2$ ground-state configuration for the metal-based orbitals, ionization from these three orbitals being easily identified. The ground state of $[(\eta\text{-}C_5H_4Me)TiS]_4$ cannot be unambiguously assigned from the PE spectrum. The d band region of the $[(\eta\text{-}C_5H_5)CrO]_4$ and $[(\eta\text{-}C_5H_4Me)CrO]_4$ spectra shows fewer features. In these cases the metal d electrons are localized on the Cr ions, and the diamagnetism shown at low temperatures is the result of weak antiferromagnetic coupling. Cyclic voltammetry studies on $[(\eta\text{-}C_5H_4{}^iPr)MoS]_4$, $[(\eta\text{-}C_5H_4{}^iPr)MoSe]_4$, $[(\eta\text{-}C_5H_4Me)CrS]_4$, $[(\eta\text{-}C_5H_4Me)CrSe]_4$, $[(\eta\text{-}C_5H_4Me)VS]_4$, and $[(\eta\text{-}C_5H_4Me)CrO]_4$ reveal two reversible oxidations for all of the compounds except $[(\eta\text{-}C_5H_4Me)CrO]_4$, which can sustain only one reversible oxidation, consistent with a smaller degree of metal d electron delocalization. Ultraviolet and visible spectroscopy data are presented for $[(\eta\text{-}C_5H_4{}^iPr)MoS]_4$, $[(\eta\text{-}C_5H_4{}^iPr)MoS]_4{}^+$, $[(\eta\text{-}C_5H_4Me)CrS]_4$, and $[(\eta\text{-}C_5H_4Me)CrS]_4{}^+$, in which the presence of a band in the spectra of the cations which is not observed in the spectra of the neutral molecules is attributed to a $^2A_1 \leftarrow {}^2T_2$ transition.

Introduction

Cubane clusters, which contain tetrahedral structural units of four metal atoms, M_4, and four non-metal atoms, E_4, combined to give an approximately cubic moiety, M_4E_4, have been the subject of extensive chemical and physical studies.[1,2] Much of the stimulus for such work comes from the occurrence of Fe_4S_4 clusters in metalloenzymes such as ferrodoxins,[3] where they act as electron-transfer agents. Many of the simpler related chemical systems act as electron storage reservoirs showing an extensive range of oxidation states.[4]

Another, perhaps more tenuous but nevertheless intellectually stimulating, consideration is the recognition that the M_4E_4 unit is the basic building block of the rock salt structure. The wide variety of electronic properties, such as conductivity and magnetism, shown by transition metal oxides with this structure[5] must be intrinsically interpretable in terms of the interaction of metal atoms in such a unit. Thus a detailed study of the electronic structure of cubane clusters such as is possible for molecules could be illuminating in a broader context.

The series of cubane clusters that we have chosen for our photoelectron (PE) spectroscopic investigation is that where the metal is also bound to a cyclopentadienyl ligand, namely $[(\eta\text{-}C_5H_4R)ME]_4$, the members of which are potentially volatile enough for gas-phase measurement. Many members of this extensive series were first synthesized by Dahl, who, following the discovery of their redox properties, demonstrated and interpreted some very interesting structure–electron number relationships.[4]

Photoelectron spectroscopy (PES) has proved a valuable tool in the investigation of compounds with metal–metal bonds and metal clusters. Since the number of observable bands tends to be that of the number of occupied valence orbitals, detailed information may be obtained on various ion states. With the

[†] Inorganic Chemistry Laboratory.
[‡] SERC Daresbury Laboratory.
[§] University of Illinois.

(1) Berg, J. M.; Holm, R. H. *Iron-Sulphur proteins*; Spiro, T. G., Ed.; Wiley-Interscience: New York, 1982; Vol. 4.
(2) Bottomley, F.; Sutin, L. *Adv. Organomet. Chem.* **1988**, *28*, 339.
(3) Holm, R. H.; Ciurli, S.; Weigel, J. A. *Proc. Inorg. Chem.* **1990**, *38*, 1.
(4) (a) Simon, G. L.; Dahl, L. F. *J. Am. Chem. Soc.* **1973**, *95*, 2164. (b) Simon, G. L.; Dahl, L. F. *J. Am. Chem. Soc.* **1973**, *95*, 2175. (c) Wei, C. H.; Wilkes, G. R.; Treichel, P. M.; Dahl, L. F. *Inorg. Chem.* **1966**, *5*, 900. (d) Trinh-Toan; Teo, B. K.; Ferguson, J. A.; Meyer, T. J.; Dahl, L. F. *J. Am. Chem. Soc.* **1977**, *99*, 408. (e) Trinh-Toan; Fehlhammer, W. P.; Dahl, L. F. *J. Am. Chem. Soc.* **1977**, *99*, 402.
(5) Goodenough, J. B. *Prog. Solid State Chem.* **1971**, *5*, 143.

0020-1669/92/1331-3779$03.00/0

more conventional technique of absorption spectroscopy, the many overlapping bands in such large molecules tend to be less informative.

The dependence of photoionization cross sections on photon energy provides a great deal of information on electronic structure. Synchrotron radiation gives access to a wide range of photon energies for PE experiments, facilitating more thorough investigations than He I/He II PES can provide. PES on gas-phase transition metal compounds over an extensive photon energy range has demonstrated significant differences between metal and ligand cross section behavior for $M(CO)_6$ (M = Cr, Mo, W),[6] $M(\eta\text{-}C_5H_5)_2$ (M = Fe, Ru, Os),[7a] and $U(\eta\text{-}C_8H_8)_2$.[7b] Such studies have also proved fruitful in probing metal–ligand bonding and changes in electronic structure on ionization of transition metal complexes in the solid state.[8] Relative partial photoionization cross sections (RPPICS) of ligand bands are mainly characterized by a rapid, monotonic decline with increasing photon energy, whereas the RPPICS of metal bands show a slower decline and a wealth of features. Study of such cross sections enables the localization of an ionizing electron to be probed.

Bonding models have been proposed, and theoretical calculations have been carried out for the cyclopentadienyl clusters.[5,9-11] The relevant results from these are presented in the Discussion.

We have undertaken a systematic study of the electronic structure of the cyclopentadienyl clusters, using PES, cyclic voltammetry, and other physical techniques, as well as some simple molecular orbital (MO) calculations. Preliminary accounts of part of this work have been reported previously.[12,13]

Experimental Section

Sample Preparation. $[(\eta\text{-}C_5H_5)CrO]_4$, $[(\eta\text{-}C_5H_4Me)CrO]_4$,[9a] and $[(\eta\text{-}C_5H_4{}^iPr)MoS]_4$[12] were prepared according to the literature methods.

$[(\eta\text{-}C_5H_4Me)CrS]_4$. $[(\eta\text{-}C_5H_4Me)_2Cr]$ (1.75 g, 8.33 mmol) was dissolved in THF (120 mL) in a 500-mL Schlenk tube. The tube was evacuated, leaving the solution under its own vapor pressure. The solution was then saturated with H_2S gas at room temperature. The color of the solution changed from crimson to black almost immediately, and gas was evolved. After half an hour, the solvent was removed under reduced pressure, and the residue was extracted with boiling petroleum ether (bp 100–120 °C). Black crystals appeared when the solution was cooled at −80 °C for 12 h. The black needle-shaped crystals were washed with cold pentane and dried under reduced pressure. Yield: 0.67 g, 49%. Anal. Calcd for $Cr_4S_4C_{24}H_{28}$: C, 44.8; H, 4.29; Cr, 30.8. Found: C, 44.2; H, 4.5; Cr, 30.8. ^1H NMR (C_6D_6): δ 4.85 (16 H); 1.83 (12 H). IR: 1489 (w), 1243 (w), 1032 (w), 803 (m), 612 cm^{-1} (w).

$[(\eta\text{-}C_5H_4Me)VS]_4$. $[(\eta\text{-}C_5H_4Me)_2V]$ was treated with H_2S in the manner described above. After 1 h the solution turned from violet to dark blue. After 72 h the solution had become dark brown/black. THF was removed under reduced pressure, and the residue heated under reduced pressure at 60 °C for 2 h to sublime unreacted $[(\eta\text{-}C_5H_4Me)_2V]$ onto a liquid-nitrogen-cooled probe. The black-brown product was extracted into toluene and crystallized from the solution at −80 °C for 12 h. The fine needles produced were washed with cold toluene and dried under reduced pressure. Characterization provided evidence of half a mole of toluene of crystallization per mole of vanadium cluster. Anal. Calcd for $V_4S_4C_{24}H_{28}$: C, 44.65; H, 4.35. Calcd for $V_4S_4C_{24}H_{28} + {}^1/_2(C_7H_8)$: C, 47.55; H, 4.64. Found: C, 48.43; H, 4.70. Mass spectrum, *m/e*: found, 648; calcd for $V_4S_4C_{24}H_{28}{}^+$, 648.

$[(\eta\text{-}C_5H_4Me)CrSe]_4$ and $[(\eta\text{-}C_5H_4{}^iPr)MoSe]_4$ were synthesized in a manner similar to the sulfur analogues.[14] **$[(\eta\text{-}C_5H_4Me)TiS]_4$** was prepared by the literature method.[15]

$[(\eta\text{-}C_5H_4Me)CrS]_4PF_6$. $[(\eta\text{-}C_5H_4Me)CrS]_4$ (0.3 g) was dissolved in toluene (20 mL) and reacted with iodine (0.06 g) dissolved in toluene (10 mL). On addition of iodine a very fine suspension was formed. The solvent was removed under reduced pressure and the residue dissolved in warm acetone (25 mL), forming a brown/black solution. This solution was reacted with an aqueous solution (10 mL) of NH_4PF_6. A black precipitate was formed after removal of most of the acetone under reduced pressure. The precipitate was isolated and recrystallized from ethanol at −80 °C. Anal. Calcd for $C_4S_4C_{24}H_{28}PF_6$: C, 36.1; H, 3.50. Found: C, 36.1; H, 3.51.

$[(\eta\text{-}C_5H_4{}^iPr)MoS]_4BF_4$ was prepared by the literature method.[12]

Photoelectron Spectra. He I and He II PE spectra were obtained using a PES Laboratories 0078 spectrometer interfaced with a RML 380Z microprocessor. Spectra were calibrated with reference to He, Xe, and N_2. The temperatures at which data were collected are given in Table I. The highest kinetic energy band in the He I spectra with an apparent IE of 4.99 eV is a He self-ionization peak, due to the ionization of He atoms by He II radiation. The He I spectrum of $[(\eta\text{-}C_5H_4{}^iPr)MoS]_4$ shown in Figure 4c was obtained using a Perkin-Elmer PS16 spectrometer in order to avoid the presence of the He self-ionization line inevitably present in spectra acquired with the PES Laboratories 0078 spectrometer.

Table I. Measurement Temperatures for the He I and He II Spectra

compound	temp (°C) He I	temp (°C) He II
$[(\eta\text{-}C_5H_4Me)VS]_4$	220	225
$[(\eta\text{-}C_5H_4Me)TiS]_4$	176	176
$[(\eta\text{-}C_5H_4Me)CrS]_4$	170	170
$[(\eta\text{-}C_5H_4Me)CrO]_4$	140	140
$[(\eta\text{-}C_5H_4Me)CrSe]_4$	228	242
$[(\eta\text{-}C_5H_4{}^iPr)MoS]_4$	195	231
$[(\eta\text{-}C_5H_4{}^iPr)MoSe]_4$	195	207

During the course of measurement of $[(\eta\text{-}C_5H_4Me)VS]_4$, some toluene was evolved at ca. 80 °C. The spectrum obtained subsequently between 200 and 220 °C was assumed to be that of the solvent-free cubane cluster.

We also attempted to obtain PE spectra of $[(\eta\text{-}C_5H_5)FeS]_4$ and $[(\eta\text{-}C_5H_4Me)CoS]_4$. Although some results were obtained, the spectral profile changed with time suggesting decomposition of the sample and so the results are not presented here.

RPPICS and PE branching ratios (BR) were determined for $[(\eta\text{-}C_5H_4{}^iPr)MoS]_4$ using synchrotron radiation in the photon energy range 21–80 eV. A full account of the experimental method that we employ at Daresbury has been given,[6] and the apparatus and its performance is described elsewhere;[16] therefore only a brief account of experimental procedures is given here.

Synchrotron radiation from the 2-GeV electron storage ring at the SERC's Daresbury Laboratory was monochromated using a toroidal grating monochromator (TGM) and was used to photoionize gaseous samples in a cylindrical ionization chamber. The photoelectrons were energy analyzed with a three-element zoom lens in conjunction with a hemispherical electron energy analyzer which was positioned at the "magic angle" in order to eliminate the influence of the PE asymmetry parameter, β, on signal intensity. This angle is dependent on the polarization of the radiation and varies with photon energy. The polarization varied from 74% to 94% over the photon energy range employed, and the "magic angle" for each $[(\eta\text{-}C_5H_4{}^iPr)MoS]_4$ and inert gas spectrum was adjusted

(6) Cooper, G.; Green, J. C.; Payne, M. P.; Dobson, B. R.; Hillier, I. H. *J. Am. Chem. Soc.* **1987**, *109*, 3836.
(7) (a) Cooper, G.; Green, J. C.; Payne, M. P. *Mol. Phys.* **1988**, *63*, 1031. (b) Brennan, J. G.; Green, J. C.; Redfern, C. M. *J. Am. Chem. Soc.* **1989**, *111*, 2373.
(8) (a) Didziulis, S. V.; Cohen, S. L.; Gerwith, A. A.; Solomon, E. I. *J. Am. Chem. Soc.* **1988**, *110*, 250. (b) Butcher, K. D.; Didziulis, S. V.; Briat, B.; Solomon, E. I. *J. Am. Chem. Soc.* **1990**, *112*, 2231. (c) Butcher, K. D.; Gebhard, M. S.; Solomon, E. I. *Inorg. Chem.* **1990**, *29*, 2067.
(9) (a) Bottomley, F.; Paesz, D. E.; White, P. S. *J. Am. Chem. Soc.* **1982**, *103*, 5581. (b) Bottomley, F.; Grein, F. *Inorg. Chem.* **1982**, *21*, 4170.
(10) (a) Bolinger, C. M.; Rauchfuss, T. B.; Wilson, S. R. *J. Am. Chem. Soc.* **1982**, *104*, 7313. (b) Bolinger, C. M.; Rauchfuss, T. B.; Rheingold, A. L. *J. Am. Chem. Soc.* **1983**, *105*, 6321. (c) Rauchfuss, T. B.; Weatherill, T. D.; Wilson, S. R.; Zebrowski, J. P. *J. Am. Chem. Soc.* **1983**, *105*, 6508. (d) Rauchfuss, T. B.; Bolinger, C. M.; Weatherill, T. D.; Rheingold, A. L.; Wilson, S. R. *Inorg. Chem.* **1986**, *25*, 634.
(11) Williams, P. D.; Curtis, D. *Inorg. Chem.* **1986**, *25*, 4562.
(12) Bandy, J. A.; Davies, C. E.; Green, J. C.; Green, M. L. H.; Prout, C. K.; Rodgers, D. P. S. *J. Chem. Soc., Chem. Commun.* **1983**, 1395.
(13) Davies, C. E.; Green, J. C.; Stringer, G. H. *Quantum Chemistry: The Challenge of Transition Metals and Coordination Chemistry*; Veillard, A., Ed.; D. Reidel Publishing Co.: Dordrecht, The Netherlands, 1986; p 413.
(14) Baird, P.; Bandy, J. A.; Green, M. L. H.; Hamnett, A.; Marseglia, E.; Obertelli, D.; Prout, K.; Qin, J. *J. Chem. Soc., Dalton Trans.* **1991**, 2377.
(15) Darkwa, J.; Boyd, P. D. W.; Rauchfuss, T. B.; Rheingold, A. L. *J. Am. Chem. Soc.* **1988**, *110*, 141.
(16) Potts, A. W.; Novak, I.; Quinn, F.; Marr, G. V.; Dobson, B. R.; Hillier, I. H. *J. Phys. B* **1985**, *18*, 3177.

accordingly. The "magic angle" used varied from 116 to 119°. Multiple scan PE spectra were collected at each photon energy required. The decay of the storage ring beam current was corrected for by linking the scan rate with the output from a photodiode positioned to intersect the photon beam after it had passed through the gas cell. The sensitivity of the photodiode to different radiation energies was determined by measuring the np^{-1} PE spectra of Ne, Ar and Xe. These were also used to characterize and correct for a fall off in analyzer collection efficiency at kinetic energies <15 eV. Photoionization cross sections for the rare gases were taken from the literature.[17,18]

The sample, introduced into the chamber in a naphthalene-plugged tube, was sublimed into the gas cell by heating with Semflex noninductively wound heating wire. A liquid-nitrogen-cooled cold finger collected the used sample. Pressure fluctuations of the sample were corrected for by collecting a "standard" calibration spectrum before and after each data spectrum. The intensities of the bands in these spectra were then used as a relative measure of the sample density in the ionization region.

The spectra were deconvoluted by fitting both symmetric and asymmetric peaks to the PE bands. The most reliable method for obtaining band areas proved to be fitting symmetric Gaussian curves, the best fit being determined by the method of least squares. The band positions were fixed relative to one another during the fits.

The BR data are independent of both the sensitivity of the photodiode to photon energy and the long-term variation in sample pressure and are corrected only by kinetic energy calibration. Thus at kinetic energies >15 eV, the only errors are statistical. For the points on the RPPICS plots, where pressure variations and photodiode calibration factors also contribute to the possible errors, relative values of points within 5 eV of each other are probably accurate to within 5%, whereas data separated by >20 eV contain a relative uncertainty of 10%.

Ultraviolet/Visible Spectra. The UV absorption spectra of $[(\eta\text{-}C_5H_4{}^iPr)MoS]_4$ and $[(\eta\text{-}C_5H_4{}^iPr)MoS]_4{}^+$ (as $[(\eta\text{-}C_5H_4{}^iPr)MoS]_4{}^+BF_4{}^-$) were obtained, in acetone solution, using a Perkin-Elmer 330 UV spectrometer. Those of $[(\eta\text{-}C_5H_4Me)CrS]_4$ and $[(\eta\text{-}C_5H_4Me)CrS]_4{}^+$ (as $[(\eta\text{-}C_5H_4Me)CrS]_4{}^+PF_6{}^-$) were obtained, in the solid state, using the same equipment.

Cyclic Voltammetry. The dc cyclic voltammetry experiments were carried out using an Oxford Electrodes Potentiostat with a built-in waveform generator. The three-chamber electrochemical cell used had platinum electrodes. Measurements were carried out in tetrahydrofuran (THF) solution with 0.2–0.5 M $[^tBuN]^+[PF_6]^-$ as the supporting electrolyte apart from $[(\eta\text{-}C_5H_4{}^iPr)MoS]_4$, which was also studied in dimethylformamide (DMF) solution using Et_4NClO_4 as the supporting electrolyte. The reference couple was PtO/Pt for $[(\eta\text{-}C_5H_4Me)VS]_4$, $[(\eta\text{-}C_5H_4Me)CrS]_4$, and $[(\eta\text{-}C_5H_4Me)CrO]_4$, but the studies of $[(\eta\text{-}C_5H_4{}^iPr)MoSe]_4$ and $[(\eta\text{-}C_5H_4Me)CrSe]_4$ employed the ferrocene/ferrocenium couple as reference (achieved by adding a little ferrocene to the sample solution). $[(\eta\text{-}C_5H_4{}^iPr)MoS]_4$ was studied using both the PtO/Pt and ferrocenium/ferrocene couples as references.

Magnetic Measurements. The magnetic behavior of $[(\eta\text{-}C_5H_4Me)CrS]_4{}^+PF_6{}^-$ was investigated, using an Oxford Instruments Faraday Balance, over the temperature range 4.2–40 K.

Molecular Orbital Calculations. Extended Hückel molecular orbital (EHMO) calculations were performed.[19] The calculations were iterative, with the weighted H_{ij} formula. The extended Hückel parameters and the interatomic distances used are given in Table II.

Results and Discussion

Summary of Structural Information. Figure 1a shows an idealized view of the structure of the cyclopentadienyl cubane clusters under investigation. In Table III we summarize some selected distances and bond angles available on the cyclopentadienyl cubane clusters. For the M_4S_4 clusters of the early transition metals that we are investigating, the metal–metal distances largely fall within a range compatible with metal–metal bonding.[20] Also the M–S–M and S–M–S angles show that the cube is distorted with the metal atoms being pulled toward the center indicating that they are bonded together. In contrast, the structure of $[(\eta\text{-}C_5H_5)CrO]_4$ shows the cube to be distorted in the opposite direction, with the metal atoms displaced away from one another.

Dahl has discussed the changes in metal–metal distances with electron number evident in the Fe and Co compounds.[5] They are substantial, and interpretable in terms of the degree of population of antibonding orbitals. In contrast, the Mo–Mo distances vary

Table II. Atomic Parameters and Interatomic Distances[a] Used in the EHMO Calculations

atom	orbital	exponent	initial H_{ii} (eV)	d-orbital coeffs c_1	d-orbital coeffs c_2
H	1s	1.300	−13.60		
C	2s	1.625	−21.40		
	2p	1.625	−11.40		
O	2s	2.275	−32.30		
	2p	2.275	−14.80		
S	3s	2.122	−20.00		
	3p	1.827	−11.00		
Se	4s	2.440	−20.50		
	4p	2.070	−14.40		
Cr	4s	1.700	−8.66		
	4p	1.700	−5.24		
	3d	4.950 1.600	−11.22	0.4876	0.7205
Mo	5s	1.956	−8.34		
	5p	1.900	−5.24		
	4d	4.542 1.901	−10.50	0.5876	0.5876

$[(\eta\text{-}C_5H_5)ME]_4$	M–E (Å)	M–C (Å)
Cr_4O_4	1.9360	2.2590
Cr_4S_4	2.2480	2.2590
Cr_4Se_4	2.3680	2.2590
Mo_4S_4	2.3430	2.3480

[a] All C–H distances = 0.9100 Å.

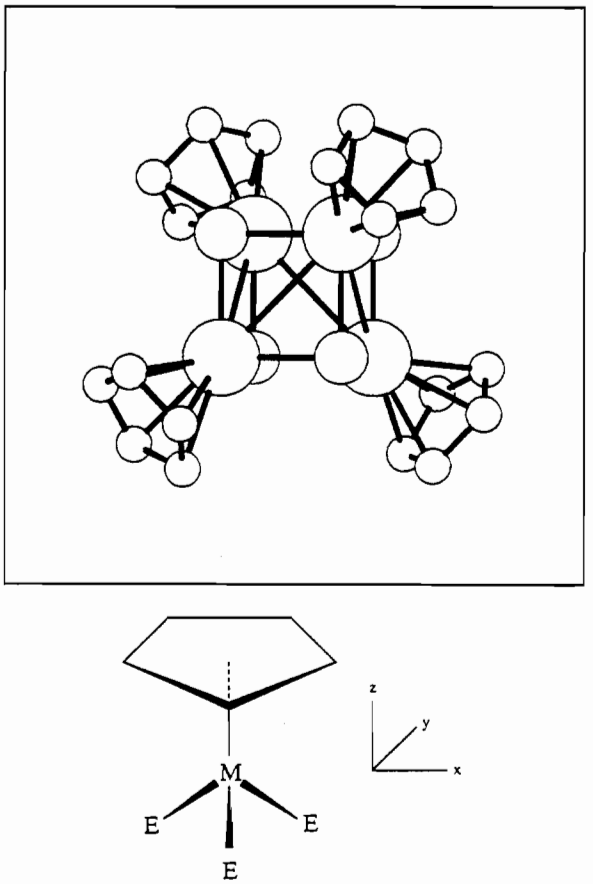

Figure 1. (a) Top: Idealized structure of the cyclopentadienyl cubane clusters omitting hydrogen atoms for clarity. (b) Bottom: Local coordinate system for a $M(\eta\text{-}C_5H_5)E_3$ unit.

(17) West, J. B.; Marr, G. V. *Proc. R. Soc. London, A* **1976**, *349*, 347.
(18) West, J. B.; Morton, J. *At. Data Nucl. Data Tables* **1978**, *22*, 103.
(19) Hoffman, R.; Lipscomb, W. N. *J. Chem. Phys.* **1962**, *36*, 2179.
(20) Cotton, F. A.; Walton, R. A. *Multiple bonds between metal atoms*; Wiley: New York, 1982.

Table III. Selected Distances and Angles Reported for Cubane Clusters

(i) Distances (Å)

compound	M–M	M–E	M–ring
$[(\eta\text{-}C_5H_4{}^iPr)MoS]_4$[12]	2.912 (1) (×2)	2.344 (2)	2.357 (8)
	2.892 (1)		2.355 (7)
	2.902 (1) (×2)		
	2.905 (1)		
	2.904 (3)[a]		
$[(\eta\text{-}C_5H_4{}^iPr)MoS]_4{}^+BF_4{}^-$[12]	2.893 (1)	2.343 (3)	2.360 (12)
	2.887 (1)		2.346 (9)
	2.860 (1)		2.339 (7)
	2.900 (1)		2.346 (9)
	2.901 (1)		
	2.923 (1)		
	2.894 (8)[a]		
$[(\eta\text{-}C_5H_4{}^iPr)MoS]_4{}^{2+}(I_3{}^-)_2$[12]	2.861 (1)	2.343 (2)	2.335 (13)
	2.902 (1)		2.340 (12)
	2.897 (1)		2.319 (18)
	2.820 (1)		2.329 (12)
	2.790 (1)		
	2.879 (1)		
	2.858 (18)[a]		
$[(\eta\text{-}C_5H_5)CrO]_4$[9]	2.900 (6)	1.9734 (4)	1.920
	2.897 (5)		
	2.841 (6)		
	2.811 (6)		
	2.712 (2)		
	2.702 (6)		

compound	M–M	M–E	M–C
$[(\eta\text{-}C_5H_4Me)CrS]_4$[31]	2.848 (2) (×2)	2.248 (2)	2.240 (9)
	2.822 (2) (×2)		
	2.822 (2) (×2)		
$[(\eta\text{-}C_5H_4Me)VS]_4$[10]	2.873 (3)[a]	2.295 (3)[a]	2.28 (1)[a]
$[(\eta\text{-}C_5H_4Me)VS]_4{}^+BF_4{}^-$[10]	2.854 (5)[a]	2.284 (5)[a]	2.25 (3)[a]
$[(\eta\text{-}C_5H_4Me)TiS]_4$[16]	2.98 (2)[a]	2.36 (2)[a]	2.37 (5)[a]

(ii) Angles (deg)

compound	M–M–M	M–E–M	E–M–E
$[(\eta\text{-}C_5H_4{}^iPr)MoS]_4$	60.0 (2)	76.3 (2)	102.2 (3)
$[(\eta\text{-}C_5H_4{}^iPr)MoS]_4{}^+$	60.0 (4)	75.2 (4)	103.0 (5)
$[(\eta\text{-}C_5H_4Me)VS]_4$		78.5 (1)[a]	101.0 (1)[a]
$[(\eta\text{-}C_5H_4Me)VS]_4{}^+$		77.3 (2)[a]	101.3 (2)[a]
$[(\eta\text{-}C_5H_4Me)TiS]_4$		77.6[1]	101.2[1]

[a] Mean values.

little between $[(\eta\text{-}C_5H_4{}^iPr)MoS]_4$, $[(\eta\text{-}C_5H_4{}^iPr)MoS]_4{}^+$, and $[(\eta\text{-}C_5H_4{}^iPr)MoS]_4{}^{2+}$, suggesting that the electrons which are being removed are nonbonding. It is perhaps significant that although the esd of the Mo–Mo distances are low for all three species, a wider range of distances is found in the di- and monocations than in the neutral molecule, indicating that there is some distortion on ionization. The data for $[(\eta\text{-}C_5H_4Me)VS]_4$ and $[(\eta\text{-}C_5H_4Me)VS]_4{}^+$ show a similar small change on ionization, and the range of distances in $[(\eta\text{-}C_5H_4Me)VS]_4{}^+$ is of a comparable size with that in $[(\eta\text{-}C_5H_4Me)VS]_4$.

The metal–metal distances decrease along the series $[(\eta\text{-}C_5H_4Me)TiS]_4$, $[(\eta\text{-}C_5H_4Me)VS]_4$, and $[(\eta\text{-}C_5H_4Me)CrS]_4$ as might be expected from the size of the metal atoms involved. The Mo–Mo distance in $[(\eta\text{-}C_5H_4{}^iPr)MoS]_4$ is about 0.07 Å larger than the Cr–Cr distance in $[(\eta\text{-}C_5H_4Me)CrS]_4$, whereas their difference in covalent radii is over 0.1 Å, indicative of greater metal–metal bonding in the second-row transition metal system. On going from $[(\eta\text{-}C_5H_4Me)CrS]_4$ to $[(\eta\text{-}C_5H_5)CrO]_4$, the average Cr–Cr distance decreases by only 0.02 Å which, given that the covalent radii of S and O are 1.04 and 0.74 Å, respectively,[21] provides evidence that the metal–metal interaction in the Cr:O cluster is weak.

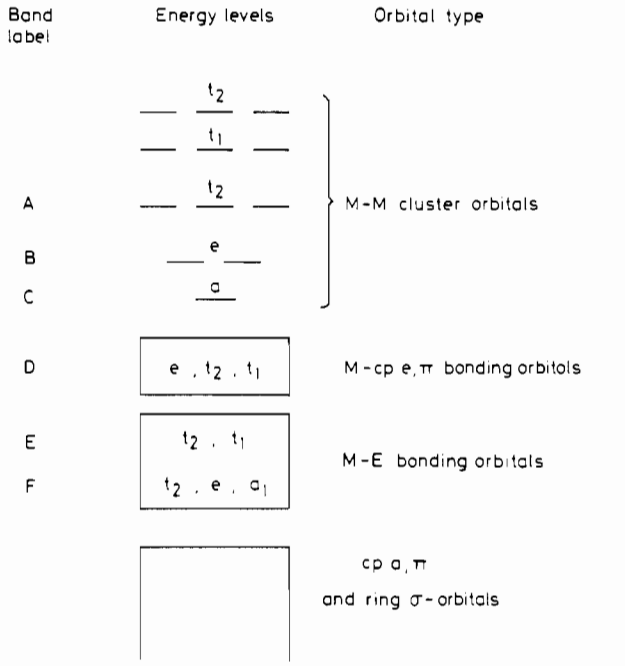

Figure 2. Schematic MO diagram for a cyclopentadienyl cubane cluster with labels corresponding to the bands observed in the PE spectra.

Table IV. Transformational Properties of the Atomic Valence Orbitals in T_d Symmetry

orbitals considered	irreducible representations
cyclopentadienyl pπ	
a_1	$A_1 + T_2$
e_1	$E + T_1 + T_2$
chalcogen p	
p_z	$A_1 + T_2$
$(p_x + p_y)$	$E + T_1 + T_2$
metal d,s,p	
s, p_z, d_{z^2}	$A_1 + T_2$
$(p_x + p_y)$, $(d_{xz} + d_{yz})$, $(d_{xy} + d_{x^2-y^2})$	$E + T_1 + T_2$

Bonding: Preliminary Considerations. For the purpose of assigning the PE spectra, it is useful to present a bonding model for these cubane clusters in which the interaction of the metal atoms with the cyclopentadienyl rings, with the chalcogen atoms, and with each other are initially treated separately and in a semilocalized manner. We will deal first with the "framework" of the cluster, namely the bonds between the cubane atoms along the cube edges, and the binding of the cyclopentadienyl ligands, and subsequently with the interactions between the metal atoms. The T_d symmetry group is used for orbital labeling; this assumes that the metal–cyclopentadienyl centroid axis is one of infinite rotation, an approximation made in many treatments.[22]

The basis set in which we are interested contains the cyclopentadienyl pπ orbitals, the chalcogen p orbitals and the metal valence orbitals. We neglect the σ-structure of the rings, which is largely unperturbed on bonding to the metal, and also the s orbitals of the chalcogens. These have ionization energies of 28.48 (O), 20.20 (S), and 20.15 eV (Se) and may be regarded as core orbitals for our purposes. The transformational properties of the valence orbitals are given in Table IV and an MO diagram derived from these orbitals is presented in Figure 2. The E *n*p derived symmetry orbitals interact with the appropriate metal symmetry orbitals to produce bonding and antibonding combinations. The 12 bonding molecular orbitals are all filled and are responsible for binding the framework of the cubane unit. Metal–cyclopentadienyl (Cp) bonding is generated by interaction of the e_1 Cp levels (transforming as $e_1 + t_1 + t_2$ in the T_d point group)

(21) Pauling, L. *The nature of the chemical bond*; Cornell University Press: Ithaca, NY, 1960.

(22) Evans, S.; Green, J. C.; Jackson, S. E.; Higginson, B. *J. Chem. Soc., Dalton Trans.* **1974**, 304.

with the appropriate metal symmetry levels (largely d_{xz} and d_{yz} derived). Eight bonding and eight antibonding orbitals again result, and all of the former are filled. The four ring a_1 π orbitals are also filled. Thus 48 of the cluster valence electrons are involved in M–E and M–Cp bonding, leaving the Cr and Mo clusters 12 electrons to accomodate in metal based orbitals, the V cluster 8, and the Ti cluster 4.

The group theoretical treatment tells us the symmetry of the residual metal orbitals, and we can gain further insight into their nature by looking into the interactions of the $(\eta\text{-}C_5H_5)ME_3$ unit, which has the extensively investigated "piano-stool" structure.[23] In the local axis system indicated in Figure 1b, the $(\eta\text{-}C_5H_5)ME_3$ fragment has three orbitals of largely d character which are uninvolved in metal ligand bonding; these are principally d_{z^2}, $d_{x^2-y^2}$ and d_{xy} in character. When we combine the four $(\eta\text{-}C_5H_5)ME_3$ units in the cubane structure, the d_{z^2} orbitals generate MOs of a_1 and t_2 symmetry and the $d_{x^2-y^2}$ and d_{xy} pair produce orbitals of e, t_2, and t_1 symmetry. The energy ordering of these five MO sets will depend on the energy of the fragment basis orbitals as well as the interaction between the metal atoms and indeed may vary between the various cubane clusters. We may, however, guess their probable occupancy by considering the symmetry of orbitals necessary for binding fully the metal tetrahedron. The six edges of a tetrahedron transform as $a_1 + e + t_2$ so the maximum possible binding by 12 electrons would correspond to occupancy of orbitals of these symmetries. From the electron number considerations above, we see that this is possible in the cases of the Mo and Cr clusters.

The diamagnetism of the Mo clusters studied fits with an $a_1^2e^4t_2^6$ configuration for the 12 metal electrons. Also consistent with the closed shell nature of a tetrahedral species would be a variant on the above, namely $a_1^2e^4t_1^6$, or full occupancy of any pair of t symmetry orbitals, i.e. $t_x^6t_y^6$. Any other configurations would have to be distorted to achieve diamagnetism. As all the structures are perforce nontetrahedral, this latter possibility cannot be ruled out on structural grounds.

There has been much debate as to the exact ordering of the MOs which result from the interaction of the metal atoms. Bottomley and Grein, citing the paramagnetism and distortion from T_d symmetry of $[(\eta\text{-}C_5H_5)CrO]_4$, reject the bonding model outlined above.[9b] On the basis of an EHMO calculation, they suggest an orbital occupancy of $e^4t_2^6t_1^2$. EHMO calculations by Williams and Curtis on $[(\eta\text{-}C_5H_5)CrO]_4$ support an $e^4a_1^2t_2^6$ configuration,[11] and they attribute the paramagnetism and distorted structure to a small HOMO–LUMO gap.

EHMO calculations were performed on $[(\eta\text{-}C_5H_5)CrO]_4$, $[(\eta\text{-}C_5H_5)CrS]_4$, $[(\eta\text{-}C_5H_5)CrSe]_4$, and $[(\eta\text{-}C_5H_5)MoS]_4$, assuming T_d geometry for the M_4E_4 unit. Figure 3 shows representatives of the highest occupied molecular orbitals of t_2, e, and a_1 symmetry, generated by the EHMO calculation performed on $[(\eta\text{-}C_5H_5)MoS]_4$. The orbitals are heavily localized on the tetrahedron of metal atoms. Our calculations give an ordering $e < a_1 < t_2$ for $[(\eta\text{-}C_5H_5)CrO]_4$, and $e < t_2 < a_1$ for $[(\eta\text{-}C_5H_5)CrS]_4$, $[(\eta\text{-}C_5H_5)CrSe]_4$, and $[(\eta\text{-}C_5H_5)MoS]_4$. For all four clusters our calculations suggest that the 12 metal-based electrons occupy MOs that are bonding between the tetrahedron of metal atoms, an effect that decreases in the order $a_1 > e > t_2$. For the e levels, this is the only significant interaction, whereas the a_1 and t_2 have a M–E antibonding contribution as well, which is strongest for the a_1 MO. Hence the e MOs lie lowest in energy in all four calculations, and the a_1 MO is raised above the t_2 as the E atom increases in size, on account of the reduced M–M bonding and increased M–E antibonding interactions.

All of the calculations and proposed bonding models are, therefore, in agreement as to the symmetries and localization of the highest lying cluster MOs, if not as to their precise ordering.

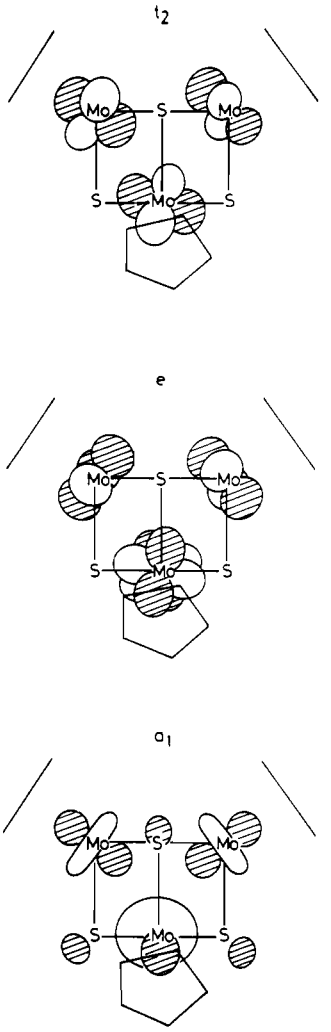

Figure 3. Representations of the t_2, e, and a_1 metal-localized orbitals.

In our experimental studies, we sought to verify the bonding model outlined above, and to obtain evidence as to the ground-state configurations and orderings of the ion states.

Assignment of the PE Spectra. The PE spectra obtained are shown in Figures 4 and 7–13. The points represent the experimental data and the solid lines a least squares fit to these points. Ionization energy data is presented in Table V together with the band assignments, which are discussed below.

$[(\eta\text{-}C_5H_4{}^iPr)MoS]_4$. PE spectra of $[(\eta\text{-}C_5H_4{}^iPr)MoS]_4$, obtained at photon energies of 33 and 51 eV using synchrotron radiation are shown in Figure 4a,b, together with band labelings. Also presented is the low binding energy region (5–10 eV—Figure 4c), obtained using HeI radiation (21.2 eV), in which the resolution is slightly superior to the spectra acquired by use of synchrotron radiation. RPPICS and BR data were obtained using synchrotron radiation over the photon energy range 21–80 eV. Table VI presents RPPICS data with statistical errors for bands A–F in the PE spectrum of $[(\eta\text{-}C_5H_4{}^iPr)MoS]_4$; BR data and statistical errors for bands A–F relative to their combined cross section are given in Table VII. RPPICS of bands A, B, and C are plotted in Figure 5a and BR for bands A, B, and C relative to the total cross section of A + B + C is plotted in Figure 5b. An assignment may be made by comparison with PE spectra of other metal cyclopentadienyl compounds[24] and on the basis of the observed cross section variations and fine structure of the bands.

One feature that is often observed in the RPPICS of metal PE bands is that of a p → d resonance. This arises when the incident photon beam excites an inner p electron, of the same primary

(23) Albright, T. A.; Burdett, J. K.; Whangbo, M. H. *Orbital interactions in chemistry*; Wiley-Interscience: New York, 1985.

(24) Green, J. C. *Struct. Bonding* **1981**, *43*, 37.

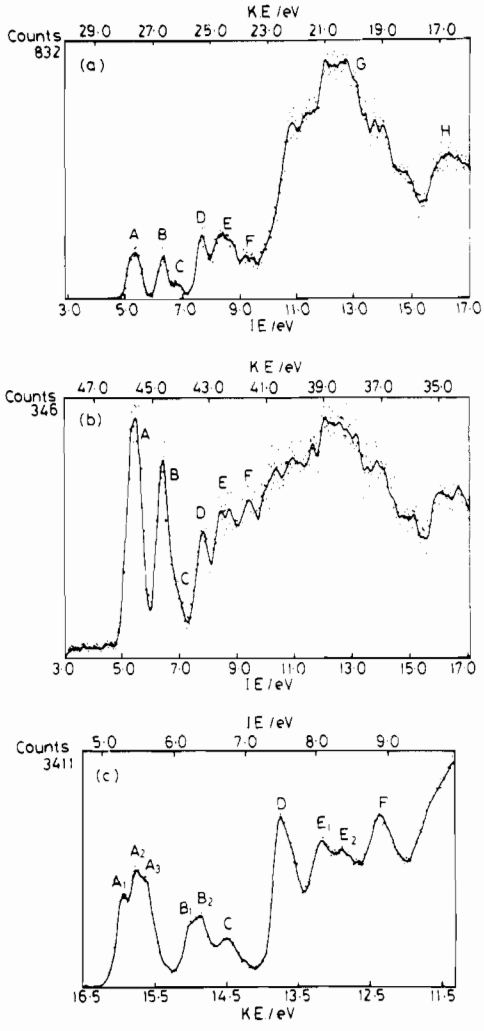

Figure 4. PE spectrum of $[(\eta\text{-}C_5H_4{}^iPr)MoS]_4$ at photon energies of (a) 33, (b) 51, and (c) 21.2 eV (He I).

quantum number as the valence d electron ionized, to an empty d level, a process favored by the angular momentum selection rule. A super-Coster–Kronig (SCK) transition may follow excitation, in which an electron falls back into the p hole and a valence d electron is ionized.[25] The advent of another channel for ionization may give rise to a substantial increase in the d photoionization cross section at such photon energies.

The Mo free atom 4p subshell ionizes at 42eV($4p_{3/2}$) and 45eV($4p_{1/2}$).[26] Thus MOs with significant Mo character would be expected to show a resonance at photon energies in this region. There is indeed an increase in the RPPICS of bands A, B, and C in the region 39–60 eV (Figure 5a), the magnitude of which decreases in the order A > B > C, suggesting a substantial Mo 4d contribution to these MOs. That the resonance feature extends to photon energies well beyond the 4p subshell ionization potentials is due largely to the very short lifetime of the intermediate in the resonance channel and the associated uncertainty as to its energy.

The 3p subshell of atomic S is calculated to have a Cooper minimum at a photon energy of 36 eV,[27] although this value has been found to alter slightly when Cooper minima have been detected in MOs having a high S content. For example, Carlson et al. have found a minimum in the photoionization cross section of the $2\pi_g^{-1}$ (HOMO) of CS_2 (an essentially S lone pair orbital) at 40 eV.[28] It is unfortunate that the Cooper minimum of S and the onset of the Mo p → d resonance should occur at around the same photon energy (35–40 eV). However, the relative magnitudes of the two phenomena allow them to be distinguished fairly easily. Resonance features are in general much larger effects than Cooper minima, and there is little doubt that the cross section increases of the first three bands are due to a Mo p → d resonance.

The PE spectra of $[(\eta\text{-}C_5H_4{}^iPr)MoS]_4$ strongly suggest that the neutral molecule has the ground-state configuration $a_1{}^2e^4t_2{}^6$. First, there are clearly three independent band systems in the low ionization energy (IE) region; second, their relative intensities suggest assignment of A to a $^2T_2$ ion state, B to a ^2E ion state, and C to a $^2A_1$ ion state; third, the structure observable on bands A and B (A shows three maxima and B two) is consistent with Jahn–Teller distortion of the $^2T_2$ and ^2E states respectively, and would be difficult to explain with any other degeneracies. The ^2E state should distort to a $^2A_1$ and a $^2B_1$ state, whereas the $^2T_2$ distorts to a $^2B_2$ and ^2E state, the latter being also Jahn–Teller active.

The BR plot (Figure 5b) indicates that all three bands show broadly similar behavior. The relative areas of bands B and C are extremely sensitive to the curve-fitting program, but it seems clear that the cross section of band C falls most rapidly at low photon energies, has the weakest resonance, and gains in relative magnitude from 60 to 80 eV. All these features suggest that this MO has the greatest S character: the fall at low photon energies corresponding to the approach to the S 3p Cooper minimum, the weaker resonance indicating a smaller Mo 4d character, and the relative gain up to 80 eV corresponding to the approach of the Mo 4d Cooper minimum. This is in agreement with the EHMO calculation. Band A has the most pronounced resonance, and its cross section falls away most rapidly at high photon energies, indicating the greatest Mo character (the Cooper minimum in the cross section of the 4d subshell of Mo is calculated to occur at a PE kinetic energy of 82 eV[27]). Band B would appear to be intermediate between the two in terms of Mo:S content, the most noticeable feature in its BR being the increase in the region 21–27 eV. This feature, which is also visible in the RPPICS plot, may well be due to a small molecular shape resonance.[29] It should be stressed, however, that although the BR differences between bands A, B, and C may be rationalized in terms of the relative Mo:S contribution to the ionizing MOs, the S contributions are small, and there is little doubt that the dominant atomic orbital (AO) component is Mo 4d.

The ^2E and $^2A_1$ states lie some distance above the $^2T_2$ state in energy, suggesting that the a_1 and e orbitals of the neutral cluster are substantially more bonding than the t_2 orbital. This is in agreement with our EHMO calculation, which suggests that the Mo–Mo bonding interaction is weakest in the t_2 orbitals. It would appear that the calculation is overemphasizing the S contribution to the t_2 and a_1 MOs, and the ordering differences between calculation ($a_1 > t_2 > e$) and experiment ($^2T_2 < {}^2E < {}^2A_1$) may be explained on these grounds. The calculation predicts Mo–Mo bonding to increase in the order $t_2 < e < a_1$, and this orbital ordering is altered only because of a Mo–S antibonding interaction in the t_2 and a_1 levels. Experiment reveals this interaction to be small and hence that the dominant effect upon orbital ordering is Mo–Mo bonding. That the t_2 orbital of $[(\eta\text{-}C_5H_4{}^iPr)MoS]_4$ is nonbonding (or even mildly antibonding) is indicated by the negligible change in Mo–Mo distance between the neutral molecule and the cations discussed above. We therefore deduce that the principal source of M–M bonding in these cubane clusters comes from the a_1 and e orbitals.

Band D has the shape and ionization energy commonly associated with ionizations from the top π orbitals of the cyclopentadienyl ring.[24] The cross section data for this band are

(25) Dehmer, J. L.; Starace, A. F.; Fano, U.; Sugar, J.; Cooper, J. W. *Phys. Rev. Lett.* **1971**, *26*, 1521.
(26) *Handbook of X-ray and Ultraviolet Photoelectron Spectroscopy*; Briggs, D., Ed.; Heyden: London, 1977.
(27) Yeh, J. J.; Lindau, I. *At. Data Nucl. Data Tables*, **1985**, *32*, 1.
(28) Carlson, T. A.; Krause, M. O.; Grimm, F. A.; Allen, J. D.; Mehaffy, D.; Keller, P. R.; Taylor, J. W. *J. Chem. Phys.* **1981**, *75*, 3288.
(29) Robin, M. B. *Chem. Phys. Lett.* **1985**, *119*, 33.

Table V. Ionization Energies (eV) of $[(\eta\text{-}C_5H_4Me)TiS]_4$, $[(\eta\text{-}C_5H_4Me)VS]_4$, $[(\eta\text{-}C_5H_4Me)CrS]_4$, $[(\eta\text{-}C_5H_4Me)CrSe]_4$, $[(\eta\text{-}C_5H_4{}^iPr)MoS]_4$, $[(\eta\text{-}C_5H_4{}^iPr)MoSe]_4$, $[(\eta\text{-}C_5H_5)CrO]_4$, and $[(\eta\text{-}C_5H_4Me)CrO]_4$

				M–M			M–C_5H_5	M–E		
M	E	R	adiabatic	$^2T_2$ band A	^2E band B	$^2A_1$ band C	e + t_1 + t_2 band D	t_2, t_1 band E	t_2, e band F_1	a_1 band F_2
V	S	Me	5.3	5.72	6.18	6.97	8.04	8.25	9.59	10.46
Cr	S	Me	5.4	5.72	6.09	6.87	7.92	8.35	9.72	10.62
Cr	Se	Me	5.41	5.74	6.21	6.79	7.81	8.56	9.24	10.23
Mo	S	^{i}Pr	5.0	5.28	6.33	6.90	7.78	8.40	9.32	
				5.48	6.47			8.65		
Mo	Se	^{i}Pr	4.88	5.17	6.12	6.73	7.76	8.12	9.95	
				5.37	6.27			8.65		
				5.51				8.91		

					M–C_5H_5	M–E		
M	E	R	adiabatic	metal d band X	D	E	F_1	F_2
Cr	O	H	6.0	6.48	8.15	8.87	10.11	
				7.05				
				7.39				
Cr	O	Me	5.9	6.32	8.02	8.65	10.09	
				6.77				
				7.29				
Ti	S	Me	5.61	5.96	8.06		9.51	10.28

Table VI. RPPICS Data for Bands A–F in the PE Spectrum of $[(\eta\text{-}C_5H_5{}^iPr)MoS]_4$

	RPPICS (arbitrary units)					
photon energy (eV)	band A	band B	band C	band D	band E	band F
21.00	34115.9 ± 468.7	17432.3 ± 339.1	12284.4 ± 286.5	41566.3 ± 532.6	73100.3 ± 713.4	68439.6 ± 697.3
24.00	19453.9 ± 292.0	11962.4 ± 231.6	6210.1 ± 167.9	22408.2 ± 322.1	44312.9 ± 457.0	32068.3 ± 392.4
27.00	14342.3 ± 256.1	10266.9 ± 216.7	3554.9 ± 127.5	13356.1 ± 248.2	27308.2 ± 357.8	15328.4 ± 270.4
30.00	11423.1 ± 192.3	7170.8 ± 152.4	3578.4 ± 107.7	10078.1 ± 180.7	21719.8 ± 265.2	9438.8 ± 174.8
33.00	6749.4 ± 134.0	4067.8 ± 104.0	1987.0 ± 727	5784.5 ± 124.1	11433.1 ± 174.5	5654.0 ± 122.7
36.00	3206.2 ± 84.4	2149.2 ± 69.0	1243.8 ± 52.5	4844.0 ± 103.7	9924.0 ± 148.4	3603.7 ± 89.4
39.00	4626.2 ± 102.7	2965.2 ± 82.2	1553.1 ± 59.5	5028.4 ± 107.0	10287.8 ± 153.1	3177.9 ± 85.1
42.00	7895.8 ± 133.6	5729.5 ± 113.8	2558.9 ± 76.0	4431.6 ± 100.1	10309.1 ± 152.6	2816.0 ± 79.8
45.00	8412.9 ± 147.4	3274.0 ± 127.3	2327.7 ± 77.5	3466.0 ± 94.6	8427.3 ± 147.5	3430.9 ± 94.1
48.00	9235.2 ± 154.7	6380.1 ± 128.6	2163.5 ± 74.9	4107.9 ± 103.2	7743.9 ± 141.7	3634.2 ± 97.1
51.00	10606.4 ± 157.9	6552.8 ± 124.1	2331.7 ± 74.0	3600.5 ± 92.0	3794.8 ± 126.4	3956.4 ± 96.4
54.00	8400.5 ± 146.7	4890.7 ± 111.9	1803.2 ± 67.9	2941.2 ± 86.8	5703.0 ± 120.8	2904.6 ± 86.2
56.00	6626.6 ± 140.7	1402.6 ± 110.7	1380.0 ± 64.2	2001.7 ± 77.3	4266.0 ± 112.9	2694.7 ± 89.7
60.00	4164.9 ± 107.0	2184.2 ± 77.5	901.8 ± 49.8	1778.0 ± 69.9	2859.2 ± 88.7	1128.4 ± 55.7
65.00	2456.5 ± 65.9	1259.3 ± 47.2	546.8 ± 31.1	1624.8 ± 53.6	2209.3 ± 62.5	759.9 ± 36.7
70.00	1992.0 ± 46.7	1036.6 ± 33.7	541.2 ± 24.3	1623.3 ± 42.2	2471.0 ± 52.0	880.9 ± 31.2
75.00	725.1 ± 24.4	436.7 ± 18.9	199.5 ± 12.8	1058.5 ± 29.5	1281.4 ± 32.4	357.8 ± 17.1
80.00	529.9 ± 18.1	306.8 ± 13.8	211.5 ± 11.5	841.4 ± 22.8	1188.1 ± 27.1	562.3 ± 18.7

Table VII. BR Data for Bands A–F in the PE Spectrum of $[(\eta\text{-}C_5H_5{}^iPr)MoS]$

	branching ratio					
photon energy (eV)	band A	band B	band C	band D	band E	band F
21.00	0.138 ± 0.002	0.070 ± 0.001	0.050 ± 0.001	0.168 ± 0.002	0.296 ± 0.003	0.277 ± 0.003
24.00	0.14 ± 0.002	0.088 ± 0.002	0.045 ± 0.001	0.164 ± 0.003	0.325 ± 0.003	0.235 ± 0.003
27.00	0.170 ± 0.003	0.122 ± 0.003	0.042 ± 0.002	0.159 ± 0.003	0.324 ± 0.005	0.182 ± 0.004
30.00	0.180 ± 0.003	0.113 ± 0.003	0.057 ± 0.002	0.159 ± 0.003	0.342 ± 0.005	0.149 ± 0.003
33.00	0.189 ± 0.004	0.114 ± 0.003	0.056 ± 0.002	0.163 ± 0.004	0.320 ± 0.006	0.158 ± 0.004
36.00	0.128 ± 0.004	0.086 ± 0.003	0.050 ± 0.002	0.194 ± 0.005	0.397 ± 0.007	0.144 ± 0.004
39.00	0.167 ± 0.004	0.107 ± 0.003	0.056 ± 0.002	0.182 ± 0.004	0.372 ± 0.006	0.115 ± 0.003
42.00	0.234 ± 0.004	0.170 ± 0.004	0.076 ± 0.002	0.131 ± 0.003	0.306 ± 0.005	0.083 ± 0.003
45.00	0.260 ± 0.005	0.194 ± 0.004	0.072 ± 0.003	0.107 ± 0.003	0.261 ± 0.005	0.106 ± 0.003
48.00	0.279 ± 0.005	0.192 ± 0.004	0.065 ± 0.002	0.123 ± 0.003	0.233 ± 0.005	0.109 ± 0.003
51.00	0.313 ± 0.005	0.194 ± 0.004	0.069 ± 0.002	0.106 ± 0.003	0.201 ± 0.004	0.117 ± 0.003
54.00	0.315 ± 0.006	0.183 ± 0.005	0.068 ± 0.003	0.110 ± 0.003	0.214 ± 0.005	0.109 ± 0.003
56.00	0.314 ± 0.007	0.195 ± 0.006	0.065 ± 0.003	0.095 ± 0.004	0.202 ± 0.006	0.128 ± 0.005
60.00	0.320 ± 0.009	0.168 ± 0.006	0.069 ± 0.004	0.137 ± 0.006	0.220 ± 0.008	0.087 ± 0.004
65.00	0.277 ± 0.008	0.142 ± 0.006	0.062 ± 0.004	0.183 ± 0.007	0.249 ± 0.008	0.086 ± 0.004
70.00	0.233 ± 0.006	0.121 ± 0.004	0.063 ± 0.003	0.190 ± 0.006	0.290 ± 0.007	0.103 ± 0.004
75.00	0.179 ± 0.007	0.108 ± 0.005	0.049 ± 0.003	0.261 ± 0.008	0.316 ± 0.009	0.088 ± 0.004
80.00	0.146 ± 0.005	0.084 ± 0.004	0.058 ± 0.003	0.231 ± 0.007	0.326 ± 0.009	0.154 ± 0.006

given in Table VI and are shown in Figure 6. It is immediately clear that there is no resonance feature similar to that shown by the first three bands, although it is possible that some small Mo contribution to the MOs is revealing itself in the way that the monotonic fall off in cross section that would be expected were the ionizing MOs purely C based appears to be halted in the resonance region (36–56 eV).

We assign bands E and F to Mo–S bonding orbitals, the framework orbitals referred to earlier. The cross section data for these bands are given in Table VI and are shown in Figure 6. As with band D, there is no indication of a large resonance feature, although differences can be seen in the behavior of the two bands. Band E shows RPPICS behavior similar to that of band D, whereas band F shows a much more rapid decrease in cross section and

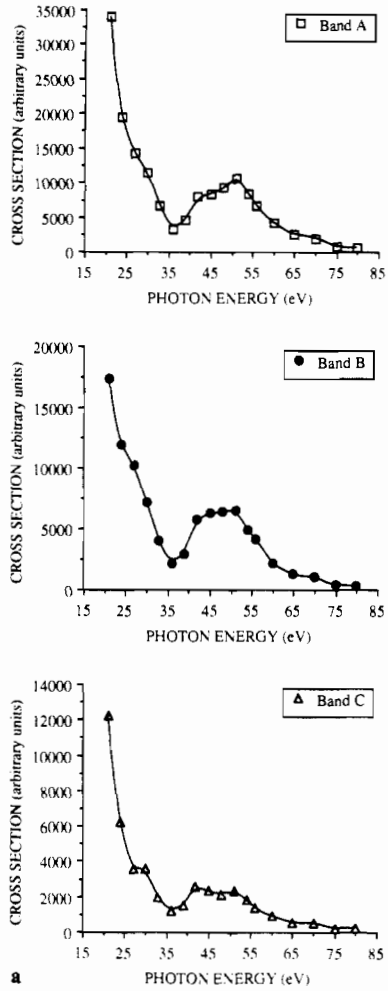

Figure 5. (a) RPPICS of bands A, B, and C in the PE spectrum of $[(\eta\text{-}C_5H_4{}^iPr)MoS]_4$. (b) BR of bands A, B and C in the PE spectrum of $[(\eta\text{-}C_5H_4{}^iPr)MoS]_4$.

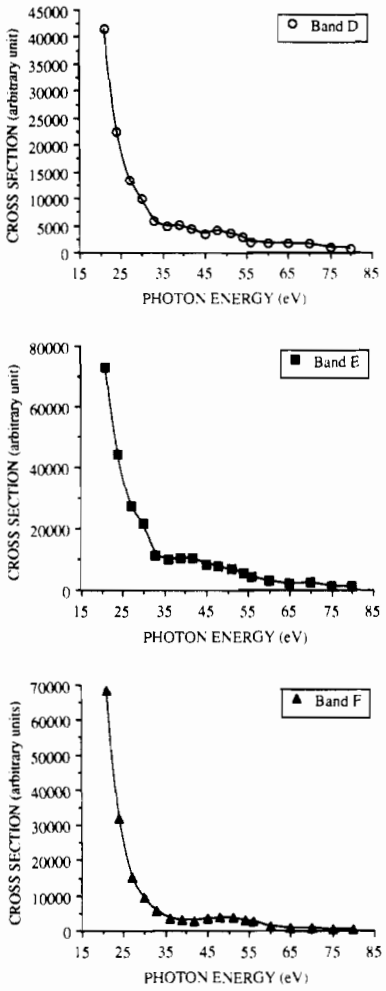

Figure 6. RPPICS of bands D, E, and F in the PE spectrum of $[(\eta\text{-}C_5H_4{}^iPr)MoS]_4$.

there is clearly a minimum in its cross section at 42 eV. The appearance of a Cooper minimum in band F strongly suggests that the orbitals ionizing under band F are more S based than those under band E. Bands E and F fall in the ionization energy window between the top $e_1\pi$ cyclopentadienyl ionization and those from the other ring orbitals. We may therefore assign bands E and F to ionization from the framework Mo–S bonding orbitals. The calculation orders the 12 Mo–S bonding orbitals

$$t_2 > t_1 > t_2 > e > a_1$$

The upper levels t_2 and t_1 have ca. 30% Mo character while the more tightly bound levels t_2, e, and a_1 have ca. 20% Mo character. This accumulation of Mo character in the upper Mo–S bonding orbitals fits with the cross section changes described above. We, therefore, assign band E to ionization from the upper t_2 and t_1 orbitals and band F to ionization from the lower t_2, e, and possibly a_1 bonding orbitals. Evidence from the PE spectrum of $[(\eta\text{-}C_5H_4Me)CrS]_4$ discussed below suggest that the a_1 ionization may lie under band G.

Bands G and H can be attributed to ionizations from C–H and C–C σ bonding orbitals localized on the cyclopentadienyl rings. The large number of orbitals ionizing in this region makes further assignment impossible, and no attempt was made to measure RPPICS and BRs for these bands.

PE Spectral Assignment of the Metal d-Band Region. The discussion of the PE spectra of the other cubane molecules studied will be divided into two sections. In the first we shall concentrate on the metal-d-based ionizations, before moving on to a consideration of the M–Cp and M–E ionization regions. The bands due to C–H and C–C σ bonding orbitals will not be discussed further.

$[(\eta\text{-}C_5H_4{}^iPr)MoSe]_4$. The PE spectrum of $[(\eta\text{-}C_5H_4{}^iPr)MoSe]_4$, shown in Figure 7, can be assigned in the same way as that of $[(\eta\text{-}C_5H_4{}^iPr)MoS]_4$ (Table V). In both cases the electron richness of the clusters is indicated by the low adiabatic IE (5.0 eV for $[(\eta\text{-}C_5H_4{}^iPr)MoS]_4$ and 4.88 eV for $[(\eta\text{-}C_5H_4{}^iPr)MoSe]_4$). The ease of oxidation of the two clusters is discussed below. Note that the adiabatic first IE of the Se cluster is lower than that of the S cluster.

$[(\eta\text{-}C_5H_4Me)CrS]_4$ and $[(\eta\text{-}C_5H_4Me)CrSe]_4$. The low-energy regions of the PE spectra of $[(\eta\text{-}C_5H_4Me)CrS]_4$ and $[(\eta\text{-}C_5H_4Me)CrSe]_4$ are shown in Figures 8 and 9, respectively. For the Cr:S cluster, three metal ionization bands can be distinguished, analogous to those found for $[(\eta\text{-}C_5H_4{}^iPr)MoS]_4$ but without the

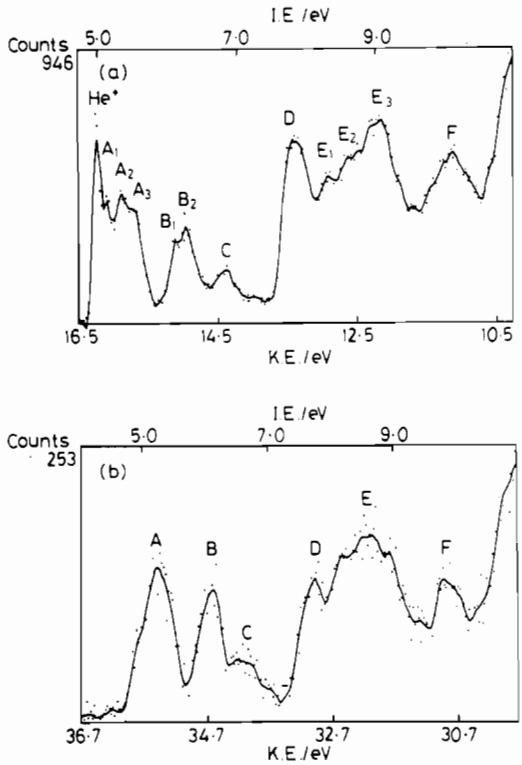

Figure 7. PE spectrum of $[(\eta\text{-}C_5H_4{}^iPr)MoSe]_4$: (a) He I; (b) He II.

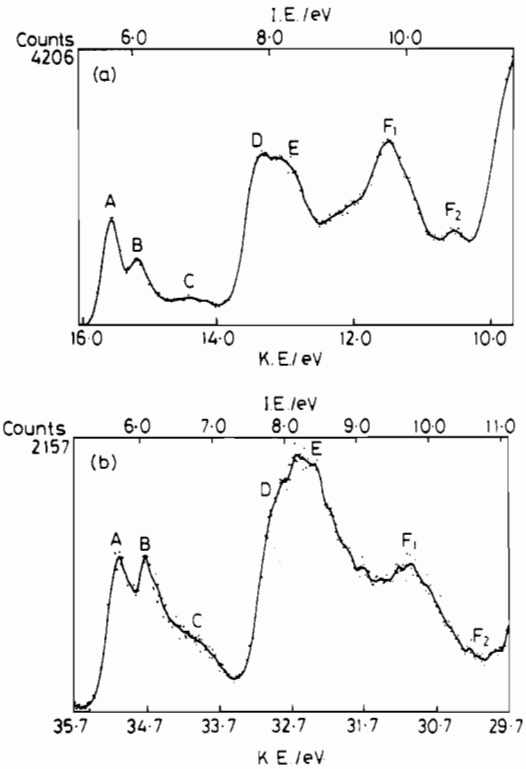

Figure 8. PE spectrum of $[(\eta\text{-}C_5H_4CH_3)CrS]_4$: (a) He I; (b) He II.

fine structure. They are assigned accordingly: band A to the $^2T_2$ ion state, band B to the ^2E state, and band C to the $^2A_1$ state. Band C is more convincingly visible in the He II spectrum than the He I spectrum. In the case of the Cr:Se cube, the metal ionizations occur over a smaller range, and it is not possible to identify three separate maxima, though the band shape is compatible with a more closed up version of the $[(\eta\text{-}C_5H_4Me)CrS]_4$ spectrum. The three values quoted in Table V are inferred from such a fit to the band profile.

The t_2 ionization energies are higher than those in the Mo analogues, indicating that the clusters are less readily oxidized.

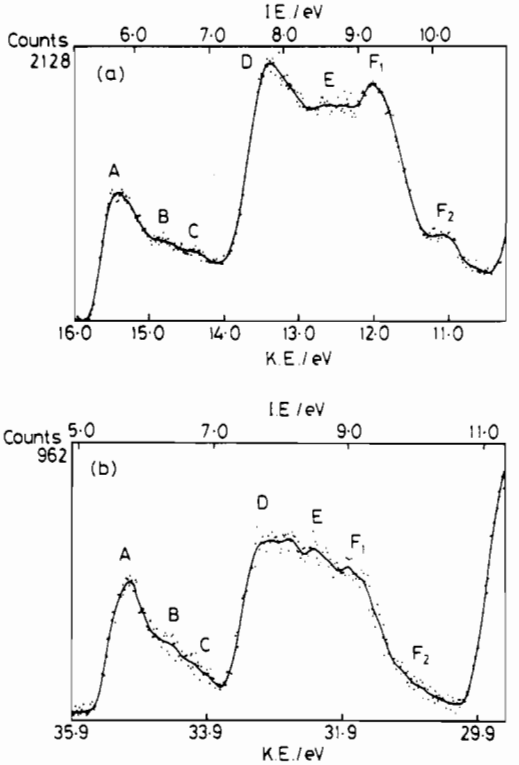

Figure 9. PE spectrum of $[(\eta\text{-}C_5H_4CH_3)CrSe]_4$: (a) He I; (b) He II.

Also the spread of metal ionization energies is less, indicating that the interaction between the metal atoms is less than is the case for the second-row transition element, a well established trend.[20] In contrast to the Mo analogues, substitution of S by Se in the cubane raises the first IE. We attribute this to the ensuing greater Cr–Cr distance and weakening of the Cr–Cr bonding, resulting in a smaller spread of orbital energies. In the Mo clusters the metal–metal bonding seems to hold up much better with increasing distance.

$[(\eta\text{-}C_5H_4Me)VS]_4$. The He I and He II spectra of $[(\eta\text{-}C_5H_4Me)VS]_4$ (Figure 10) can be assigned by comparison with those of $[(\eta\text{-}C_5H_4Me)CrS]_4$, which they resemble. The V cluster has four fewer electrons than the Cr one. Band A is of smaller relative intensity for $[(\eta\text{-}C_5H_4Me)VS]_4$ strongly suggesting that it is the associated orbital that is partially filled, and that the configuration is based on a distortion of the $a_1{}^2e^4t_2{}^2$ configuration. This concurs with the results of the Xα–SW calculation[10] which gives a ground state for the V cluster of $a_1{}^2b_1{}^2a_1{}^2e^2$. The a_1 ionization is again a broad band, overlapping with the e ionization and more apparent in the He II spectrum. The bands are less well-defined than in the Cr case, possibly as a result of exchange splitting of the orbital ionizations into doublet and quartet states. The IE of corresponding bands vary little from those of $[(\eta\text{-}C_5H_4Me)CrS]_4$; the incomplete filling of the t_2 orbitals does not seem to affect adversely the metal–metal bonding. This has also been demonstrated by the small change in metal–metal distance on oxidation.[10]

$[(\eta\text{-}C_5H_4Me)TiS]_4$. The Ti:S clusters have been shown to be diamagnetic,[15] ruling out a $^3A_2$ ground state from the configuration $a_1{}^2e^2$. The structure shows D_{2d} symmetry, with two Ti–Ti distances that are shorter than the other four, though all are within bonding range. Alternative possibilities are based on a distorted $a_1{}^2e^2$ configuration, for example $a_1{}^2b_1{}^2$, giving a singlet ground state, or based on an e^4 configuration; however, since distortion of the latter to D_{2d} symmetry also gives a $a_1{}^2b_1{}^2$ configuration, the distinction is somewhat unreal. Two localized metal–metal bonds in D_{2d} symmetry transform as $a_1 + b_2$. A b_2 orbital can be derived by distortion of the t_2 set of T_d orbitals, so this should also be considered as a possibility.

The PE spectrum of $[(\eta\text{-}C_5H_4Me)TiS]_4$, shown in Figure 11, has just one resolved metal d band. Its profile is more like those

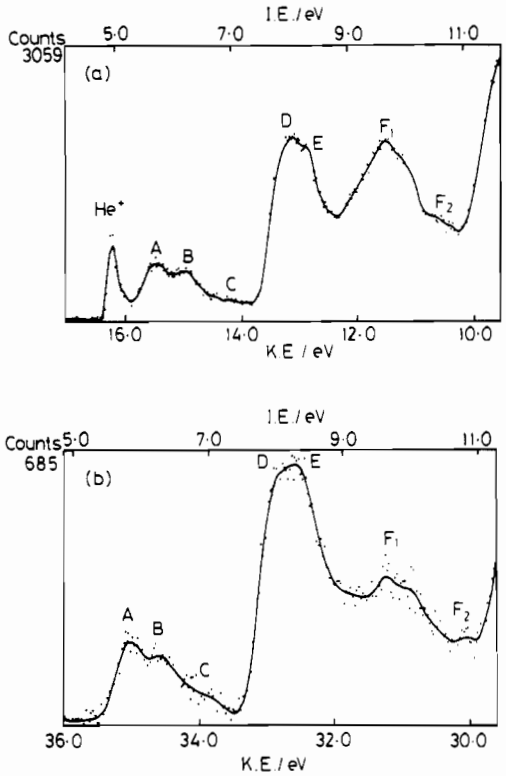

Figure 10. PE spectrum of $[(\eta\text{-}C_5H_4CH_3)VS]_4$: (a) He I; (b) He II.

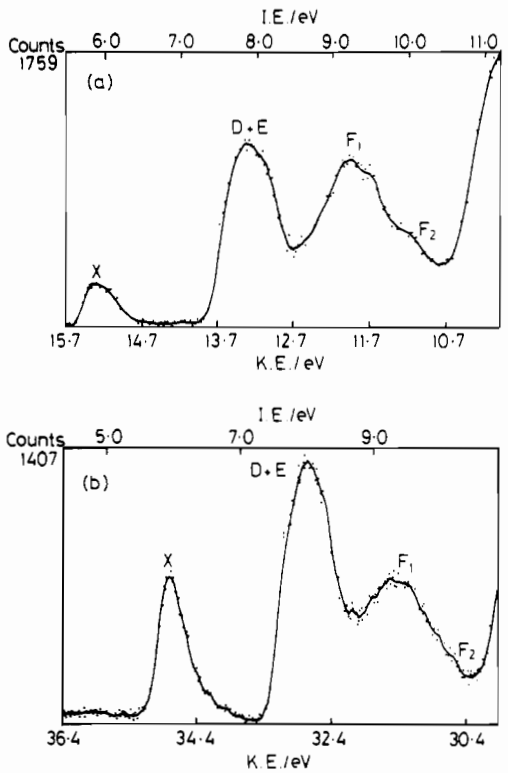

Figure 11. PE spectrum of $[(\eta\text{-}C_5H_4CH_3)TiS]_4$: (a) He I; (b) He II.

of the e ionization bands found in the other spectra than the broad flat a_1 band, suggesting that metal–metal bonding in this compound is not particularly strong. If the ground state is indeed $a_1^2b_1^2$, then the PE evidence suggests that the two MOs have very similar IEs. Asymmetry on the high IE side of the metal d band may be due to the presence of two overlapping ionizations.

$[(\eta\text{-}C_5H_5)CrO]_4$ and $[(\eta\text{-}C_5H_4Me)CrO]_4$. The PE spectra of $[(\eta\text{-}C_5H_5)CrO]_4$ and $[(\eta\text{-}C_5H_4Me)CrO]_4$ are given in Figures 12 and 13. They are very similar to one another and, in striking contrast to the M_4S_4 and M_4Se_4 clusters, show no resolved d-band

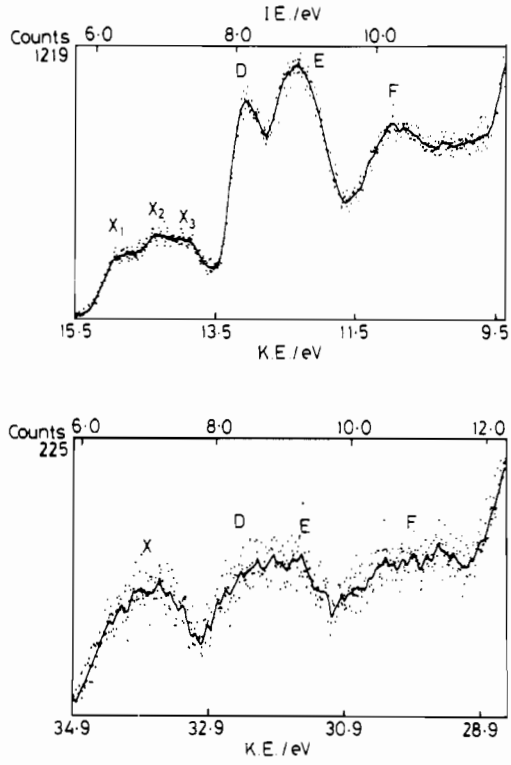

Figure 12. PE spectrum of $[(\eta\text{-}C_5H_5)CrO]_4$: (a) He I; (b) He II.

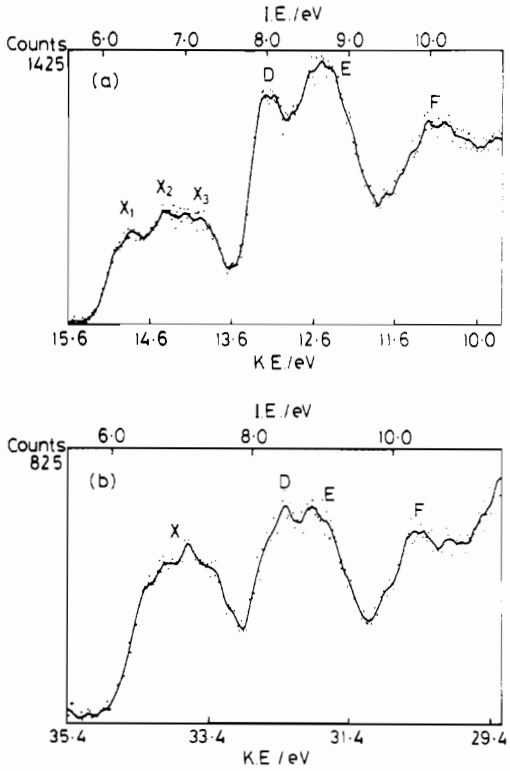

Figure 13. PE spectrum of $[(\eta\text{-}C_5H_4CH_3)CrO]_4$: (a) He I; (b) He II.

structure. We cannot, therefore, obtain an assignment of the spectra in the same way as for the M_4S_4 and M_4Se_4 compounds. These compounds have been shown to be paramagnetic at room temperature, with the effective magnetic moment reducing as the temperature is lowered. Possibly the best picture for the interaction between the metals in this case is that of weak antiferromagnetic coupling. If this is the case, a single configuration MO model for the 12 metal electrons is not very adequate as it grossly underestimates the amount of electron correlation; any reasonable MO picture must include substantial configuration interaction. The consequences of such a situation for a PE

experiment is that there is no longer a one to one correlation between the ionization bands observed and the orbitals occupied in the basic configuration. Other ion states are also observed, so called shake-up states, where, in addition to an electron being ionized, another electron may appear to have been promoted to a higher orbital. This has been observed, for example, in the ionization of the d electrons of $[Ti_2(\eta\text{-}C_5H_5)_2(\eta^5,\eta^5\text{-}C_{10}H_8)(\mu\text{-}Cl)_2]$.[30] We may therefore expect to access more than just three ion states and also observe ionization to those relating to configurations where the t_1 and upper t_2 orbitals are occupied. In the light of this, the complex manifold observed for the d band in the PE spectra of the Cr O clusters is not surprising.

If all five Cr 3d based cluster MOs are occupied in the molecular ion states giving rise to the observed d band, we have a measure of the d bandwidth in such a cluster. The experimentally determined d bandwidth of 1.6 eV is less than that found in the M_4S_4 and M_4Se_4 clusters, in which ion states involving population of the higher t_1 and t_2 orbitals are not observed. This evidence supports the idea that the d electrons in the Cr:O clusters are primarily localized on the Cr^{3+} ions, and interact only weakly with their neighbours. The structural information presented earlier supports this conclusion.

PE Spectral Assignment of the M–Cp and M–E Ionizations. In all of the spectra obtained there is a band ionizing at approximately 8 eV (band D), which has a sharp leading edge. As was mentioned in the discussion of $[(\eta\text{-}C_5H_4{}^iPr)MoS]_4$, this band is believed to be due to ionizations from the top π orbitals of the cyclopentadienyl ring. Its IE is relatively insensitive to changes in both the metal and chalcogen, with less than 0.4 eV covering the entire range. There does, however, appear to be a correlation of the IE of band D with the inductive properties of the R group attached to the cyclopentadienyl ring, for as the electron-donating power of the R substituent increases from H → Me → ^{i}Pr, the IE of band D drops, from 8.15 eV in $[(\eta\text{-}C_5H_5)CrO]_4$ to 7.76 eV in $[(\eta\text{-}C_5H_4{}^iPr)MoSe]_4$.

The region to higher IE from band D is not so simple to assign, and significant differences may be observed between the different clusters. These will be discussed individually.

$[(\eta\text{-}C_5H_4{}^iPr)MoSe]_4$. As with $[(\eta\text{-}C_5H_4{}^iPr)MoS]_4$, two bands (at 8.91 eV (band E) and 9.95 eV (band F)) may be distinguished (Figure 7). The profile of band E is different from the $[(\eta\text{-}C_5H_4{}^iPr)MoS]_4$ equivalent, the IE is somewhat greater and the lower IE components increase in relative intensity in the He II spectrum. The IE of band F is also slightly greater than that in the $[(\eta\text{-}C_5H_4{}^iPr)MoS]_4$ spectrum, and it does not fall away in intensity in the He II spectrum to the same extent as the equivalent band in $[(\eta\text{-}C_5H_4{}^iPr)MoS]_4$.

Calculations reveal that the Cooper minimum of the 4p subshell of Se is less pronounced than that of the 3p level of S and occurs at a higher photon energy (65 eV as opposed to 36 eV).[27] Hence MOs that are derived from Se 4p AOs will not show the same fall off in cross section as the incident photon energy is increased from 21.2 eV (He I) to 40.8 eV (He II) as would the equivalent S 3p based MOs. Comparison of the behavior of band F in the $[(\eta\text{-}C_5H_4{}^iPr)MoSe]_4$ spectra with band F in $[(\eta\text{-}C_5H_4{}^iPr)MoS]_4$ suggests very strongly that the MOs ionizing in this region have a significant Se contribution. The assignment of bands E and F is similar to the corresponding bands in $[(\eta\text{-}C_5H_4{}^iPr)MoS]_4$, i.e. to framework bonding MOs with differing degrees of Mo 4d character.

$[(\eta\text{-}C_5H_4Me)CrS]_4$ and $[(\eta\text{-}C_5H_4Me)CrSe]_4$. The profile of the PE bands ionizing in the 7.5–10.5-eV region in the spectrum of $[(\eta\text{-}C_5H_4Me)CrS]_4$ (Figure 8) is different from that seen in $[(\eta\text{-}C_5H_4{}^iPr)MoS]_4$ and $[(\eta\text{-}C_5H_4{}^iPr)MoSe]_4$. Band D is not so well resolved, and has a high IE component which increases in relative intensity in the He II spectrum. The shape, position and He I/He II behavior of the band at 9.72 eV lead us to suggest that this corresponds to band F of the $[(\eta\text{-}C_5H_4{}^iPr)MoS]_4$ and $[(\eta\text{-}C_5H_4{}^iPr)MoSe]_4$ spectra and hence that band E has moved to a lower IE and is now almost coincident with band D. A new, previously unobserved band (band F_2) is visible at 10.62 eV, the He I/He II behavior of which suggests that the MOs giving rise to it have localization properties similar to those ionizing under band F, i.e., are largely S-based framework bonding orbitals.

It is a feature common to all of the R = H and R = Me cluster spectra that the main band of C–C and C–H σ bonding MO ionizations is slightly higher in IE than in the R = ^{i}Pr case. This effect, which is due to a combination of the relative inductive properties of the R groups and the greater number of C–C and C–H bonding MOs in the ^{i}Pr substituent, reveals another PE band (band F_2) which is obscured in the ^{i}Pr cluster spectra. We assign band F_2 to the a_1 M–E framework orbital.

$[(\eta\text{-}C_5H_4Me)CrSe]_4$ (Figure 9) is similar to $[(\eta\text{-}C_5H_4Me)CrS]_4$, except that the region between bands D and F is not so well resolved. This is especially so in the He II spectrum, in which only one band is observed. It would seem that band E is not as close to band D in the $[(\eta\text{-}C_5H_4Me)CrSe]_4$ spectrum, but is intermediate between bands D and F. By analogy with the other cubane spectra, we expect band E to gain in relative intensity in the He II spectrum and band F to fall (although to a lesser extent than in the S clusters). The result of these two effects is a single, broad band.

3d AOs are radially less extended than 4d, and it is therefore expected that the bonding interaction between M and E atoms is greater for Mo than Cr, resulting in a greater stabilization of the framework MOs in the Mo clusters. The changes in the IE of band E would appear to confirm this.

$[(\eta\text{-}C_5H_4Me)VS]_4$ and $[(\eta\text{-}C_5H_4Me)TiS]_4$. The shape, position and He I/He II behavior of bands D–F in the spectrum of $[(\eta\text{-}C_5H_4Me)VS]_4$ (Figure 10) are similar to $[(\eta\text{-}C_5H_4Me)CrS]_4$, and may be explained in the same way.

The situation is not so clear cut in $[(\eta\text{-}C_5H_4Me)TiS]_4$ (Figure 11). There are only two bands in the region 7.5–10.5 eV, with the band at higher IE having a shoulder at 10.28 eV. In the He II spectrum, the band at 8.06 eV increases in relative intensity with respect to the band at 9.51 eV, and the size of the increase indicates that it is not only Cp π orbitals that are giving rise to this ionization. Given that the band at 9.51 eV is characteristic of the F bands in the other spectra studied, it may well be that band E is coincident with band D in this spectrum. The IE difference between bands D and E thus increases from ~0 eV in $[(\eta\text{-}C_5H_4Me)TiS]_4$ to 0.21 eV in $[(\eta\text{-}C_5H_4Me)VS]_4$ and 0.43 eV in $[(\eta\text{-}C_5H_4Me)CrS]_4$. This progressive stabilization of the M:S framework MOs arises because the IE of the metal 3d AOs increases from Ti to Cr, giving a better energy match with the S 3p valence AOs and enhanced stabilisation of the resultant MOs.

$[(\eta\text{-}C_5H_5)CrO]_4$ and $[(\eta\text{-}C_5H_4Me)CrO]_4$. The spectra of $[(\eta\text{-}C_5H_5)CrO]_4$ (Figure 12) and $[(\eta\text{-}C_5H_4Me)CrO]_4$ (Figure 13) are very similar to one another in IE, band profile, and He I/He II behavior. Three bands may be distinguished between 7.5 and 10.5 eV, and these are assigned in a manner analogous to the M:S and M:Se spectra. The main difference between the spectra of the O clusters and those of the heavier chalcogens is the He II behavior of band F (insofar as it can be distinguished in the He II spectrum of $[(\eta\text{-}C_5H_5)CrO]_4$). There is no relative intensity decrease of band F in the O cluster spectra; indeed, a slight gain relative to bands D and E is observed. This is because there is no radial node in the wavefunction of a 2p AO and consequently no Cooper minimum in its photoionization cross section. Thus MOs with large O 2p character do not show the same cross section

(30) Green, J. C.; Rankin, R.; Seddon, E. A.; Teuben, J. H.; Jonkman-Beuker, A. H.; De Boer, D. K. G. *Chem. Phys. Lett.* **1981**, *82*, 92.
(31) Kurbanov, T. K.; Lindeman, S. V.; Novotortsev, V. M.; Pasynskii, A. A.; Rakitin, T. V.; Shklover, V. E.; Struckov, Y. T. *J. Organomet. Chem.* **1983**, *248*, 309.

Table VIII. $E_{1/2}$ (V) for the First and Second Oxidation Waves of the Cubane clusters

compound	1st oxidation	2nd oxidation
$[(\eta\text{-}C_5H_4Me)VS]_4$[a]	−0.65	0.13
$[(\eta\text{-}C_5H_4Me)CrS]_4$[a]	−0.52	0.31
$[(\eta\text{-}C_5H_4Me)CrO]_4$[a]	−0.52	0.25[b]
$[(\eta\text{-}C_5H_4{}^iPr)MoSe]_4$[c]	−0.91	−0.32
$[(\eta\text{-}C_5H_4{}^iPr)MoS]_4$[c]	−0.82	−0.22
$[(\eta\text{-}C_5H_4Me)CrSe]_4$[c]	−0.66	−0.06

[a] Values measured with respect to PtO/Pt and quoted with respect to ferrocenium/ferrocene by taking the latter as being 0.84 V vs PtO/Pt. [b] Irreversible wave. [c] Values measured directly with respect to ferrocenium/ferrocene.

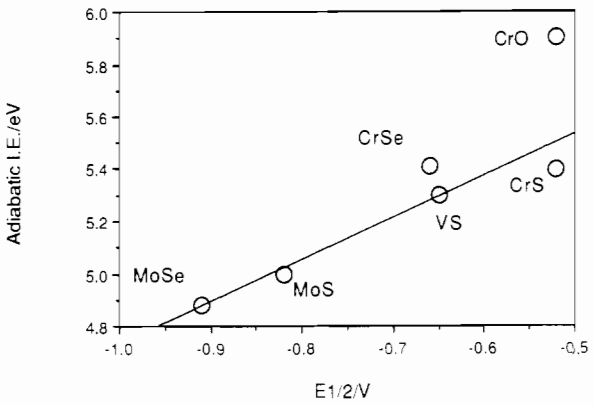

Figure 14. Plot of adiabatic IE versus $E_{1/2}$.

fall off with increasing photon energy as do S-based MOs (or, to a lesser extent, Se-based ones).

Cyclic Voltammetry Studies. $[(\eta\text{-}C_5H_4Me)VS]_4$, $[(\eta\text{-}C_5H_4Me)CrS]_4$, $[(\eta\text{-}C_5H_4{}^iPr)MoS]_4$, $[(\eta\text{-}C_5H_4Me)CrSe]_4$, $[(\eta\text{-}C_5H_4{}^iPr)MoSe]_4$ and $[(\eta\text{-}C_5H_4Me)CrO]_4$ have been studied using cyclic voltammetry. All of the compounds underwent two reversible oxidations except for $[(\eta\text{-}C_5H_4Me)CrO]_4$, in which the second oxidation led to spontaneous disassembly of the cluster. The data obtained are given in Table VIII. There is a strong correlation between the first IE (as measured by PES) and the ease of oxidation of the compounds (see Figure 14).

As the chalcogen is changed from S to Se in the ^{i}PrCpMo:E clusters, the first IE decreases and the compound becomes easier to oxidize. This can be rationalized by a consideration of the relative electronegativities of S and Se. A similar explanation may be given to account for the greater ease of oxidation of the Mo:S clusters over those of the first-row transition metals, although the greater electron-donating effect of the ^{i}Pr group over the Me may also be a factor. The slight increase in the first IE and first $E_{1/2}$ values of the Cr:S cluster when compared with the V cluster is almost certainly another example of the same effect, given the lower 3d IE and electronegativity of V over Cr.

The trends in the $E_{1/2}$ values of the second oxidations are the same as those observed in the first. That the relative difficulty of removing an electron from the monocations is similar to that from the neutral species provides further evidence that the HOMOs are similar in all of the clusters studied.

The M_4S_4 and M_4Se_4 clusters undergo two successive reversible oxidations, which is a manifestation of the delocalized nature of the metal electrons in the species. The positive charge generated on oxidation can be dispersed over the whole cluster. In contrast, the Cr_4O_4 cluster can sustain only one reversible oxidation, and we take this to be further evidence of the more localized bonding in this compound. The small d band width and insensitivity of the Cr–Cr distance to chalcogen atom changes of the Cr:O clusters are in agreement with the electrochemical data.

Visible and Ultraviolet Spectra. The bands in a PE spectrum represent the energies of the molecular ion states relative to one another. From the observed PE spectra of both $[(\eta\text{-}C_5H_4{}^iPr)MoS]_4$ and $[(\eta\text{-}C_5H_4Me)CrS]_4$ we would expect to find bands in the absorption spectra of the monocations, due to excitation from the $^2T_2$ ground state to either the ^2E or $^2A_1$ excited states, that are not present in the absorption spectra of the neutral molecule.

In both cases a band was observed in the spectrum of the cation that was not present in the spectrum of the neutral molecule. This occured at 12 900 cm^{-1} (1.6 eV) in $[(\eta\text{-}C_5H_4{}^iPr)MoS]_4^+$ and at 7000 cm^{-1} (0.87 eV) in $[(\eta\text{-}C_5H_4Me)CrS]_4^+$. This energy gap corresponds, in both cases, most closely with the separation of the adiabatic IEs of the $^2T_2$ and $^2A_1$ bands in the PE spectra. The lower frequency of the transition in $[(\eta\text{-}C_5H_4Me)CrS]_4^+$ is in agreement with the observation of a narrower spread of metal IEs in the PE spectrum of $[(\eta\text{-}C_5H_4Me)CrS]_4$, for the reasons given earlier.

By definition, the monocation is a mixed valency compound. Absorption bands in the near infrared region in such compounds are often assigned to intravalence transitions, with the valences localized in the experimental time scale. In this case, however, the occurrence of such a band is entirely consistent with a delocalized orbital model for bonding within the cluster.

Magnetic Measurements. The susceptibility measurements on $[(\eta\text{-}C_5H_4CH_3)CrS]_4PF_6$ may be fitted to the expression

$$\chi = C/(T + \Theta)$$

with a value for the Curie constant of 0.560 J^2 T^{-2} and the Weiss temperature Θ of 6.48 K. The correlation coefficient is 0.998. At higher temperatures the results can be interpreted in terms of the Curie–Weiss law, with a magnetic moment of 1.96 μ_B at 40 K, consistent with one unpaired electron. Deviation is observed at lower temperatures, which could be due to magnetic ordering at 2 K. The magnetic measurements indicate thermal population of a state with orbital angular momentum as the temperature is raised, consistent with a ^2B ground state and a thermally accessible ^2E excited state.

Summary

Our experimental investigations into the electronic structure of the M_4E_4 cubane clusters have revealed that the highest occupied molecular orbitals are metal based in all cases. The adiabatic first IE of the M_4E_4 (where M = Ti, V, Cr, and Mo and E = S and Se) is very low, consistent with the postulate that the HOMO is essentially nonbonding between the tetrahedron of metal atoms. Structural data on the M–M distances in both the neutral molecules and the mono- and dications support this assertion. Further evidence is provided by the cyclic voltammetry results, in which all of the M_4S_4 and M_4Se_4 clusters are seen to undergo two reversible oxidations. There is an excellent correlation between the $E_{1/2}$ values obtained by cyclic voltammetry and the first IE as measured by PES.

The weight of PE evidence favors a molecular ion state ordering of $^2T_2 < {}^2E < {}^2A_1$ for these clusters. The ultraviolet/visible spectra of $[(\eta\text{-}C_5H_4{}^iPr)MoS]_4^+$ and $[(\eta\text{-}C_5H_4Me)CrS]_4^+$ contain bands which are not present in the spectra of the neutral molecules, and which are consistent with $^2A_1 \leftarrow {}^2T_2$ transitions.

RPPICS data on the t_2, e, and a_1 bands in the PE spectrum of $[(\eta\text{-}C_5H_4{}^iPr)MoS]_4$ indicate the presence of a p $\rightarrow$ d giant resonance in the region 39–60 eV. This resonance is strongest for the t_2 set of MOs and weakest in the a_1 set, but is clear evidence of large Mo 4d character in all of the highest lying MOs. BR data on these three bands suggest that the a_1 MO has the greatest amount of S character, in agreement with the EHMO calculation but that it is not a large contribution. EHMO calculations appear to place too much emphasis on a M–E antibonding interaction, and this raises the energy of the a_1 MO relative to that of the e and t_2 MOs. The experimental evidence is that the S content of these orbitals is small.

In contrast to the clusters of the heavier chalcogens, the low-binding-energy region of the PE spectra of $[(\eta\text{-}C_5H_5)CrO]_4$ and

$[(\eta\text{-}C_5H_4Me)CrO]_4$ is a broad, unresolved band. The bandwidth is narrower than the spread of metal-based ionizations in the M_4S_4 and M_4Se_4 spectra and is taken to indicate that the metal electrons are more localized in the Cr_4O_4 systems. Structural data on $[(\eta\text{-}C_5H_5)CrO]_4$ and the cyclic voltammetry data on $[(\eta\text{-}C_5H_4Me)CrO]_4$, in which only one reversible oxidation is found, agree with this hypothesis.

In all of the PE spectra obtained, there is a band at ~8 eV, the IE of which varies little between compounds. This band is assigned to the top π orbitals of the Cp rings, which the RPPICS data on $[(\eta\text{-}C_5H_4{}^iPr)MoS]_4$ supports. Some correlation between the IE of band D and the inductive properties of the R group attached to the Cp ring is found, with the IE of band D in the ^iPrCp clusters generally being lower than those of the R = Me or R = H clusters.

The next ionization region is assigned to the framework MOs that are responsible for binding the cubane unit. Two ionization bands are distinguished (bands E and $F_1 + F_2$), and the RPPICS data on $[(\eta\text{-}C_5H_4{}^iPr)MoS]_4$ and the He I/He II behavior of the other compounds suggests that band F (or $F_1 + F_2$) is almost pure chalcogen np in character, whereas some slight metal nd contribution to the MOs ionizing under band E may be distinguished. Differences in the behavior of bands F as the chalcogen is varied can be readily explained by a consideration of the cross section behavior of the chalcogen *n*p AOs.

The position of band E is sensitive to changes in the metal atom, reinforcing the idea that there is some metal d character to this band. Moving from Ti → V → Cr increases the IE of band E in the M_4S_4 clusters, and a similar effect is found when the metal is altered from Cr to Mo in the M_4S_4 and M_4Se_4 clusters. These effects are interpreted in terms of the radial extension of the metal *n*d and chalcogen *n*p AOs involved in bonding and of their relative energies.

Acknowledgment. We thank the People's Republic of China (J.Q.) and the SERC for financial support and the machine staff at Daresbury for their efficient running of the SRS.

Registry No. $[(\eta\text{-}C_5H_4{}^iPr)MoS]_4$, 89389-51-5; $[(\eta\text{-}C_5H_4{}^iPr)MoSe]_4$, 118732-40-4; $[(\eta\text{-}C_5H_4{}^iPr)MoS]_4BF_4$, 89389-53-7; $[(\eta\text{-}C_5H_4Me)CrS]_4$, 86811-68-9; $[(\eta\text{-}C_5H_4Me)CrSe]_4$, 118732-42-6; $[(\eta\text{-}C_5H_4Me)TiS]_4$, 111237-35-5; $[(\eta\text{-}C_5H_4Me)VS]_4$, 93347-79-6; $[(\eta\text{-}C_5H_4Me)CrO]_4$, 86811-69-0; $[(\eta\text{-}C_5H_5)CrO]_4$, 79417-63-3; $[(\eta\text{-}C_5H_4Me)CrS]_4PF_6$, 106369-87-3; $[(\eta\text{-}C_5H_4Me)_2Cr]$, 12146-92-8; $[(\eta\text{-}C_5H_4Me)_2V]$, 12146-93-9.